

# Adsorption–Desorption Rate of Nonpolar Volatile Organic Compounds onto Activated Carbon Exemplified by C<sub>6</sub>H<sub>6</sub> and CCl<sub>4</sub>

C. L. Chuang<sup>1</sup>; P. C. Chiang<sup>2</sup>; E. E. Chang<sup>3</sup>; and C. P. Huang<sup>4</sup>

**Abstract:** This investigation was to evaluate the performance of a thermodynamic model using nonlinear driving force in conjunction with the Langmuir model exemplified by the adsorption of benzene and carbon tetrachloride onto activated carbon in mono- and binary-adsorbate systems. Results show that model-fitted adsorption and desorption rate constants could well predict the adsorption isotherms and breakthrough curves under various conditions. This numerical model can provide adsorption and desorption rate constants. The kinetic parameters are of the same order of magnitude as reported in several studies. Under high reaction temperatures, both the adsorption and desorption rate constants increased while equilibrium constants decreased. A dimensionless valuable  $C_0/K$  can be used to describe the relationship between adsorbate and adsorbent, and predict the service cycle during the adsorption process. For adsorption in binary mixtures, a high inlet concentration or a low temperature, the weak adsorbate, C<sub>6</sub>H<sub>6</sub>, will have a high breakthrough concentration when the strong adsorbate, CCl<sub>4</sub>, began to break through.

**DOI:** 10.1061/(ASCE)1090-025X(2003)7:3(148)

**CE Database subject headings:** Activated carbon; Adsorption; Desorption; Kinetics.

## Introduction

Activated carbon has been used extensively as an adsorbate for the removal of hazardous air pollutants. Major parameters affecting the adsorption process include the surface properties of the activated carbon, the characteristics and concentration of volatile organic compounds (VOCs), temperature, and humidity. King and Do (1996) used the Fourier transfer infrared technique to evaluate the effect of temperature on the adsorption capability of ethane, propane, and *n*-butane on activated carbon. They reported that the equilibrium time at high temperatures was shorter than that at low temperatures. Wood (1992) observed good correlation between molar polarization of adsorbent and adsorption capacity using the Dubinin/Radushkevich model. Other researchers (Jonas and Rehm 1972; Vahdat et al. 1995) considered the activated carbon bed adsorption process as a first-order reaction and found the Wheeler equation to be successful for application to several organic gases.

Most adsorption studies were conducted at a specific temperature. Major adsorption models used include the linear driving force (LDF) approximation (Crittenden and Weber 1978; Malek et al. 1995; Malek and Farooq 1996, 1997; Vahdat 1997), the empirical method (Yoon and Nelson 1984); and the thermodynamic equilibrium approach (Myers and Prausnitz 1965) (Table 1). The LDF method considers the adsorption process as an irreversible reaction, and the reaction rate is governed by the difference between the temporal and the equilibrium concentrations of the gas adsorbate. The LDF method is based on an isothermal plug-flow system with a linear equilibrium adsorption isotherm (Malek et al. 1995; Malek and Farooq 1996, 1997). Yoon and Nelson (1984) developed an empirical model to predict the breakthrough curve of activated carbon beds. Based on the thermodynamic characteristic of each solute at equilibrium, an ideal adsorbed solution theory was developed by Myers and Prausnitz (1965). The adsorption equilibrium of the gas mixture can be predicted from the individual single-gas isotherm using the Toth equation (Myers and Valenzuela 1986) and/or the Dubinin/Radushkevich equation (Dubinin 1989). The desorption behavior of carbon films was also observed based on the Arrhenius equation and thermal desorption spectroscopy (Pigram et al. 1994).

There are problems with the above methods. For example, the thermodynamic method considers the adsorption process only under equilibrium conditions. The LDF method accounts for the adsorption step only. The empirical method lacks theoretical validity. In essence, the adsorption is not truly equilibrium; both adsorption and desorption occur at the same time. The objectives of this investigation were to evaluate the performance of the thermodynamic model using nonlinear driving force exemplified by the adsorption of benzene and carbon tetrachloride onto activated carbon in mono- and binary-adsorbate systems, and to predict the adsorption isotherm and adsorption breakthrough curves under different operational conditions, such as temperature and gas concentration, as a means to determine the system service time.

<sup>1</sup>PhD Candidate, Graduate Institute of Environmental Engineering, National Taiwan Univ., 71 Chou-Shan Rd., Taipei, Taiwan. E-mail: clc\_chuang@ms69.url.com.tw

<sup>2</sup>Professor, Graduate Institute of Environmental Engineering, National Taiwan Univ., 71 Chou-Shan Rd., Taipei, Taiwan. E-mail: pccchiang@ccms.ntu.edu.tw

<sup>3</sup>Professor, Dept. of Biochemistry, Taipei Medical Univ., 250 Wu-Hsing St., Taipei, Taiwan. E-mail: eechang@mail.tmu.edu.tw

<sup>4</sup>Professor, Dept. of Civil and Environmental Engineering, Univ. of Delaware, Newark, DE 19716. E-mail: huang@mail.ce.udel.edu

Note. Discussion open until December 1, 2003. Separate discussions must be submitted for individual papers. To extend the closing date by one month, a written request must be filed with the ASCE Managing Editor. The manuscript for this paper was submitted for review and possible publication on May 20, 2002; approved on March 21, 2003. This paper is part of the *Practice Periodical of Hazardous, Toxic, and Radioactive Waste Management*, Vol. 7, No. 3, July 1, 2003. ©ASCE, ISSN 1090-025X/2003/3-148–155/\$18.00.

**Table 1.** Adsorption Models

Column adsorption model	Typical model equation
Linear driving force (LDF) approximation	$-D_L \frac{\partial^2 C}{\partial L^2} + U \frac{\partial C}{\partial L} + \frac{\partial C}{\partial t} + \frac{1-\varepsilon}{\varepsilon} \rho_p \frac{\partial q}{\partial t} = 0$ $\frac{\partial q}{\partial t} = k(q^* - q)$
Empirical method	$t = t_{1/2} + \frac{1}{k'} \ln \left( \frac{C}{C_0 - C} \right)$ $k' = \frac{kCQ}{W_e}$ $t_{1/2} = t \text{ when } C = C_0/2$
Ideal adsorbed solution theory	$t = \frac{W_e}{CQ} \left[ W - \frac{\rho_B Q}{k} \ln \left( \frac{C_0}{C} \right) \right]$

## Experimental Method

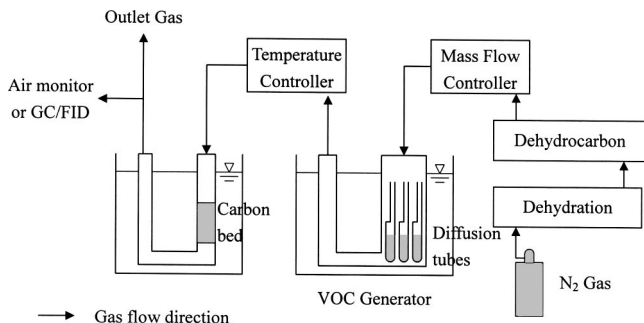
### Materials

The VOCs selected were benzene (C<sub>6</sub>H<sub>6</sub>) and carbon tetrachloride (CCl<sub>4</sub>), and the activated carbon studied was Sorbonorit 3 (Norit, the Netherlands). The activated carbon sample was of pellet form with a diameter of 3 mm and a density of 880 kg/m<sup>3</sup>. The activated carbon was ground and sieved to size between 0.35 and 0.50 mm (35–45 mesh) to prevent the wall effects. Then it was heated to 573 K in a N<sub>2</sub> atmosphere (purity 99.99%) over 24 h to desorb contaminants. The treated activated carbon was stored in a N<sub>2</sub>-filling chamber (300 K) before experiments.

Volatile organic compounds were generated by passing a stream of water and hydrocarbon-free N<sub>2</sub> gas over a series of diffusion tubes containing the pure liquid. The VOC concentrations were controlled by the number of diffusion tubes and temperature. The carrier gas flow rate was controlled at 1.2 L/min (298 K) by a mass flow meter (Instrument Inc., Sierra). The temperature of the VOC vapor was controlled by a thermostat (283–363 K) before entering the reaction column (Fig. 1). The concentrations of C<sub>6</sub>H<sub>6</sub> and CCl<sub>4</sub> studied were 8–150 and 6–300 mmol/m<sup>3</sup>, respectively.

### Adsorption in Activated Carbon Bed

For mono-VOC adsorption experiments, about 600 mg of treated activated carbon was packed in a small glass column (height=9

**Fig. 1.** Experimental apparatus

mm and cross-section area=1.76 cm<sup>2</sup>), whereas for bi-VOC experiments, the amount of treated activated carbon used was about 4,000 mg (height=60 mm and cross-section area=1.76 cm<sup>2</sup>). The column temperature was maintained at the range from 283 to 363 K for 3 h before testing. For single-component experiments, the outlet gas was continuously monitored with a portable photoionization air monitor (Perkinelmer, Photovac Model 2020). The measurements were calibrated by gas chromatography (GC) (HP 5890A; column: Supel Co., VOCOL™, No. 9354-04A) with a flame ionization detector (FID). For two-component experiments, the outlet gas was collected about 1 mL every 15 min and injected into the GC/FID for the analysis of residual organics. The detection limits of C<sub>6</sub>H<sub>6</sub> and CCl<sub>4</sub> were 100 and 30 ppm V, respectively.

## Mathematical Model

### Numerical Model Development

The following dynamic equation was used to describe the temporal mass balance of containment in question:

$$\frac{\partial C}{\partial t} - D_L \frac{\partial^2 C}{\partial L^2} + u \frac{\partial C}{\partial L} + \frac{1-\varepsilon}{\varepsilon} \rho_p \frac{\partial q}{\partial t} = 0 \quad (1)$$

where  $D_L$ ,  $C$ ,  $L$ ,  $u$ ,  $\varepsilon$ ,  $\rho$ , and  $q$ =dispersion coefficient (m<sup>2</sup>/s); concentration of VOC in the gas phase (mol/m<sup>3</sup>); length of activated carbon bed (m); gas velocity (m/s); bed void fraction; a density of activated carbon (g/m<sup>3</sup>); and adsorption capacity (g/g), respectively. By assuming the process as a nonequilibrium surface reaction and since the column is relatively short, the diffusion term can be negligible, the surface reaction rate is equal to the adsorption rate minus the desorption rate, i.e.

$$\frac{\partial \theta}{\partial t} = k_a(1-\theta)C - k_d\theta \quad (2)$$

where  $\theta$  ( $q/q_0$ )=degree of surface coverage of VOC on activated carbon surface;  $k_a$ =adsorption rate constant (m<sup>3</sup>/(s mol)); and  $k_d$ =desorption rate constant (L/s). Eq. (1) can be rewritten as

$$\frac{\partial C}{\partial t} = -U \frac{\partial C}{\partial L} - \frac{\partial \theta}{\partial t} S \quad (3)$$

where  $S$  (g/m<sup>3</sup>)=conversion factor between solid and gas phase can be further expressed by the following relation:

$$S = \frac{q_0 W}{LA - W/\rho} \quad (4)$$

It is known that the flow rate,  $Q$  (m<sup>3</sup>/s), has the following form:

$$Q = UA \left( 1 - \frac{W}{LA} \right) \quad (5)$$

where  $W$ =weight of activated carbon (g);  $A$ =cross-sectional area of the adsorption bed (m<sup>2</sup>); and  $q_0$ =maximum adsorptive capacity at the monolayer level (g/g).

Considering the activated carbon bed as an entity of  $n$  series ( $n=50$ ) of constant volume units, i.e., the physicochemical conditions within each unit are identical, and the adsorption/desorption process follows the Langmuir model. Let  $\Delta t$  (s) and  $\Delta V$  (m<sup>3</sup>) be the reaction time and the gas volume in each unit. At

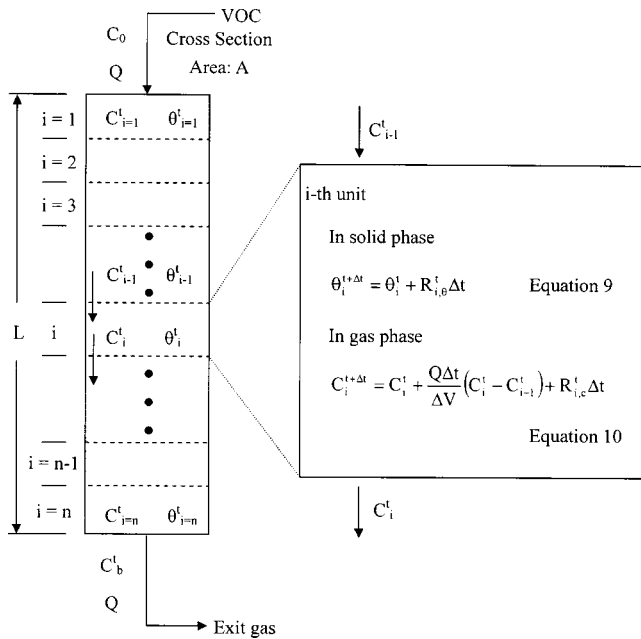


Fig. 2. Conceptual presentation of modeling approach

the  $i$ th unit and experimental time,  $t$ , the concentration change in the solid phase and the gas phase can be determined by a finite difference method.

In solid phase from Eq. (2) one has

$$\theta_i^{t+\Delta t} = \theta_i^t + [k_a(1 - \theta_i^t)C_i^t - k_d\theta_i^t] \Delta t \quad (6)$$

In the gas phase from Eq. (3), it yields

$$C_i^{t+\Delta t} = C_i^t + \frac{Q\Delta t}{\Delta V} (C_i^t - C_{i-1}^t) + [-k_a(1 - \theta_i^t)C_i^t + k_d\theta_i^t] S \Delta t \quad (7)$$

Accordingly,  $\Delta V$  can be expressed by the following equation:

$$\Delta V = \frac{LA - \frac{W}{\rho}}{n} \quad (8)$$

In the case when both VOCs are present, it is assumed that both prefer the same adsorption sites, and that a competitive adsorption process takes place.

In the solid phase, Eq. (6) becomes

$$\theta_i^{t+\Delta t, Z} = \theta_i^{t, Z} + \left[ k_a \left( 1 - \sum_Z \theta_i^{t, Z} \right) C_i^{t, Z} - k_d \theta_i^{t, Z} \right] \Delta t \quad (9)$$

In the gas phase, Eq. (7) becomes

$$C_i^{t+\Delta t, Z} = C_i^{t, Z} + \frac{Q\Delta t}{\Delta V} (C_i^{t, Z} - C_{i-1}^{t, Z}) + \left[ -k_a \left( 1 - \sum_Z \theta_i^{t, Z} \right) C_i^{t, Z} + k_d \theta_i^{t, Z} \right] S \Delta t \quad (10)$$

where  $Z=Z$ th adsorbate. Fig. 2 is the conceptual presentation of the modeling approach.

### Calculation

By definition, the equilibrium adsorption mass,  $W_e$ , and the equilibrium adsorption capacity,  $q$ , can be calculated by the following

equation:

$$q = \int_0^\infty (C_0 - C_b) Q dt / W = W_e / W \quad (11)$$

where  $C_0$  and  $C_b$  = inlet and outlet organic vapor concentrations, respectively; and  $W_e$  = equilibrium adsorption mass. With  $q$  obtained, the parameters of Langmuir ( $q_0, K_L$ ), Freundlich ( $K_F, n$ ), and Redlich-Peterson ( $K_R, B, m$ ) adsorption isotherms can be computed using the SYSTAT software package.

In numerical modeling, a series of knowns ( $\rho, A, C_0, W, L, Q$ , and  $T$ ) and estimated parameters ( $k_a$  and  $k_d$ ) were input into Eqs. (6) and (7) followed by iterative computations. The breakthrough curves were then resulted. The best fit was verified evaluating by the root mean square error method,  $\delta$ , i.e.

$$\delta = \frac{1}{C_0} \sqrt{\frac{1}{N} \sum_{n=1}^N (C_b - C')^2} \quad (12)$$

where  $C_b$ ,  $C'$ , and  $N$  = observed breakthrough concentration, calculated breakthrough concentration, and measured number in each test, respectively.

## Results and Discussion

### Determination of Reaction Parameters ( $k_a$ , $k_d$ , $E_a$ , and $E_d$ )

Table 2 shows the experimental conditions and results of a single contaminant column adsorption process, where retention time,  $\tau$ , is defined as  $(LA - W/\rho)/Q$ . The breakthrough time ( $t_b$  at  $C_b = 0.01 C_0$ ) and the exhaustion time ( $t_e$  at  $C_b = 0.99 C_0$ ) decreased significantly as temperature increased. Clearly, the model developed for the present study can reasonably predict the effluent concentration ( $\delta = 0.02 - 0.07$ ). Although both  $k_a$  and  $k_d$  increased with temperature, the equilibrium adsorption constant ( $K = k_a/k_d$ ) actually decreased. For example, the desorption rate constant of  $C_6H_6$  increased from  $1.0 \times 10^{-4}$  to  $1.1 \times 10^{-2}$  L/s as the temperature increased from 283 to 363 K; the increase in the desorption rate constant was greater than that of the adsorption rate constant [ $1.3 \times 10^{-2} - 6.0 \times 10^{-2}$  m<sup>3</sup>/(s mol)]. The equilibrium constant, however, decreased by 2 orders of magnitude (130–5.4 m<sup>3</sup>/mol) when the temperature increased from 283 to 363 K. Results also show that the equilibrium adsorption constant of  $CCl_4$  was greater than that of  $C_6H_6$ .

Based on the Arrhenius equation, the adsorption activation energy ( $E_a$ ), desorption activation energy ( $E_d$ ), adsorption frequency coefficient ( $a_a$ ), and desorption frequency coefficient ( $a_d$ ) can be calculated from the corresponding  $k_a$  and  $k_d$  values (Fig. 3). For  $C_6H_6$ , the  $E_a$  and  $E_d$  were determined to be 4.0 and 12.2 kcal/mol, respectively; the corresponding  $a_a$  and  $a_d$  values were 13 m<sup>3</sup>/(s mol) and  $2.6 \times 10^5$  L/s, individually. For  $CCl_4$ , the  $E_a$  and  $E_d$  values were 4.8 and 15.3 kcal/mol, respectively; the respective  $a_a$  and  $a_d$  values were 340 m<sup>3</sup>/(s mol) and  $4.6 \times 10^7$  L/s. Consequently, the heat of adsorption of  $C_6H_6$  and  $CCl_4$  can be determined; the values are -8.2 and -10.4 kcal/mol, respectively, for  $C_6H_6$  and  $CCl_4$ . In comparison,  $C_6H_6$  has a larger adsorption rate constant, desorption rate constant, equilibrium adsorption constant, adsorption activation energy, and desorption activation energy but a lower heat of adsorption and adsorption capacity than that of  $CCl_4$ .

**Table 2.** Adsorption Conditions, Parameters, and Statistics

VOC	Adsorption conditions and parameters		Unit Temp. (K)	Run 1 283	Run 2 303	Run 3 323	Run 4 343	Run 5 363
C <sub>6</sub> H <sub>6</sub>	Reaction conditions	Weight of carbon, <i>W</i>	g	2.001	2.005	2.001	2.002	2.001
		Length of carbon bed, <i>L</i>	cm	3	3.1	3	3	3
		Influent concentration, <i>C</i> <sub>0</sub>	mmol/m <sup>3</sup>	116	132	108	103	88
		Saturation concentration, <i>C</i> <sub>sat</sub>	mol/m <sup>3</sup>	2.6	6.3	13.5	25.8	45.1
		Flow rate, <i>Q</i>	L/min	1.14	1.2	1.3	1.38	1.46
		Breakthrough time, <i>t</i> <sub>b</sub>	min	39	27	25	22	20
		Exhaustion time, <i>t</i> <sub>e</sub>	min	130	100	90	56	38
		Retention time, $\tau$	s	$1.60 \times 10^{-1}$	$1.59 \times 10^{-1}$	$1.41 \times 10^{-1}$	$1.33 \times 10^{-1}$	$1.25 \times 10^{-1}$
	Reaction parameters	Adsorption rate constant, <i>k</i> <sub>a</sub>	m <sup>3</sup> /(s mol)	$1.3 \times 10^{-2}$	$1.6 \times 10^{-2}$	$1.9 \times 10^{-2}$	$4.0 \times 10^{-2}$	$6.0 \times 10^{-2}$
		Desorption rate constant, <i>k</i> <sub>d</sub>	L/s	$1.0 \times 10^{-4}$	$4.4 \times 10^{-4}$	$1.6 \times 10^{-3}$	$5.0 \times 10^{-3}$	$1.1 \times 10^{-2}$
		Equilibrium constant, <i>K</i>	m <sup>3</sup> /mol	130	36.6	11.7	8	5.4
	Statistics	Measured number in each test, <i>N</i>	—	27	29	41	32	26
Root mean square error, $\delta$		—	0.02	0.03	0.03	0.05	0.04	
CCl <sub>4</sub>	Reaction conditions	Weight of carbon, <i>W</i>	g	0.600	0.600	0.600	0.600	0.600
		Length of carbon bed, <i>L</i>	cm	0.9	0.9	0.9	0.9	0.9
		Influent concentration, <i>C</i> <sub>0</sub>	mmol/m <sup>3</sup>	26.8	23.7	22.5	22.2	20.6
		Saturation concentration, <i>C</i> <sub>sat</sub>	mol/m <sup>3</sup>	3.2	7.5	15.5	28.9	49.5
		Flow rate, <i>Q</i>	L/min	1.15	1.21	1.31	1.39	1.47
		Breakthrough time, <i>t</i> <sub>b</sub>	min	44	42	30	26	16
		Exhaustion time, <i>t</i> <sub>e</sub>	min	100	68	54	50	45
		Retention time, $\tau$	s	$4.70 \times 10^{-2}$	$4.46 \times 10^{-2}$	$4.14 \times 10^{-2}$	$3.89 \times 10^{-2}$	$3.68 \times 10^{-2}$
	Reaction parameters	Adsorption rate constant, <i>k</i> <sub>a</sub>	m <sup>3</sup> /(s mol)	$7.5 \times 10^{-2}$	$1.0 \times 10^{-1}$	$1.5 \times 10^{-1}$	$2.0 \times 10^{-1}$	$6.0 \times 10^{-1}$
		Desorption rate constant, <i>k</i> <sub>d</sub>	L/s	$4.0 \times 10^{-5}$	$1.1 \times 10^{-3}$	$3.0 \times 10^{-3}$	$4.8 \times 10^{-3}$	$3.1 \times 10^{-2}$
		Equilibrium constant, <i>K</i>	m <sup>3</sup> /mol	1,875	90.0	50.0	41.7	19.4
	Statistics	Measured number in each test, <i>N</i>	—	41	29	24	22	19
Root mean square error, $\delta$		—	0.04	0.07	0.02	0.02	0.03	

Note: Experimental conditions: density=880 kg/m<sup>3</sup>, bed cross-section area=1.76 cm<sup>2</sup> and *q*<sub>0</sub> 460 mg/g for C<sub>6</sub>H<sub>6</sub>, and 600 mg/g for CCl<sub>4</sub> at 303 K.

### Adsorption Isotherm

In this study, both C<sub>6</sub>H<sub>6</sub> and CCl<sub>4</sub> are nonpolar molecules; i.e., dipole moments are zero. Table 3 summarizes the results of the equilibrium adsorption capacity under various C<sub>6</sub>H<sub>6</sub> and CCl<sub>4</sub> concentrations. As expected, the equilibrium capacity increased

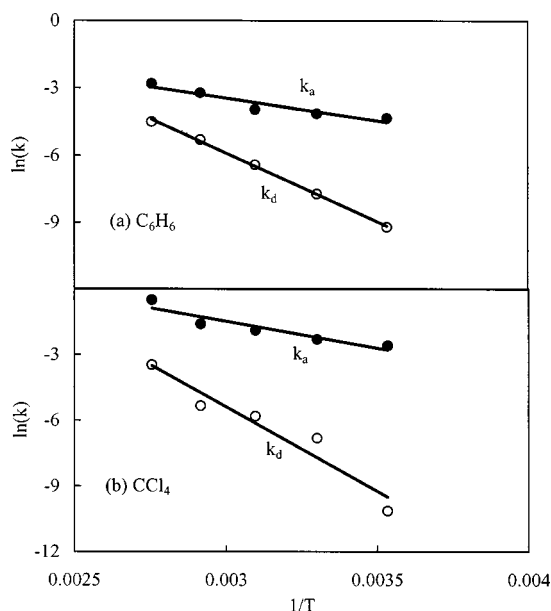


**Fig. 3.** Relationship between rate constants (*k*<sub>a</sub> and *k*<sub>d</sub>) and temperature

with the VOC concentration. The C<sub>6</sub>H<sub>6</sub> or CCl<sub>4</sub> saturation concentration (*C*<sub>sat</sub>) at a given temperature was calculated from its vapor pressure, and the adsorption capacity was plotted versus the “relative concentration” (*C*<sub>0</sub>/*C*<sub>sat</sub>) as shown in Fig. 4. All three models (Langmuir, Freundlich, and Redlich–Peterson) can reasonably describe the experimental data (*R*<sup>2</sup>=0.89–0.99). Table 4 summarizes the model parameters. The results indicate that CCl<sub>4</sub> has both high maximum adsorptive capacity and Langmuir adsorption constant (*K*<sub>L</sub>=*k*<sub>a</sub>/*k*<sub>d</sub>), which implies that CCl<sub>4</sub> is a stronger adsorbate than C<sub>6</sub>H<sub>6</sub> toward activated carbon. For the sake of convenience, the Langmuir model was chosen in subsequent numerical model analysis of the adsorption/desorption process.

Many researchers have reported that the adsorbed VOC molecules behave as a liquid phase. In this study, both C<sub>6</sub>H<sub>6</sub> and CCl<sub>4</sub> are nonpolar molecules with a liquid density of 0.885 and 1.584 g/cm<sup>3</sup>, respectively.

In principle, both the breakthrough (*t*<sub>b</sub>) and exhaustion (*t*<sub>e</sub>) time of the activated carbon decreased as the influent concentration (*C*<sub>0</sub>) and/or the reciprocal adsorption constant (*K*) increases. These phenomena were clearly demonstrated in Fig. 5, which shows that *t*<sub>b</sub> and *t*<sub>e</sub> decrease exponentially with increasing *C*<sub>0</sub>/*K*. Meanwhile, the breakthrough time of C<sub>6</sub>H<sub>6</sub> (or CCl<sub>4</sub>) will approach the exhaustion time when the *C*<sub>0</sub>/*K* reaches  $1.6 \times 10^{-2}$  (or  $4.0 \times 10^{-3}$ ). That is at exhaustion condition, influent concentration (*C*<sub>0</sub>) increases while the reaction constant (*K*) decreases and vice versa. Therefore, the dimensionless quantity *C*<sub>0</sub>/*K* not only reflects the relationship between adsorbent (*C*<sub>0</sub>)

**Table 3.** Adsorption Capacity of C<sub>6</sub>H<sub>6</sub> and CCl<sub>4</sub> onto Activated Carbon

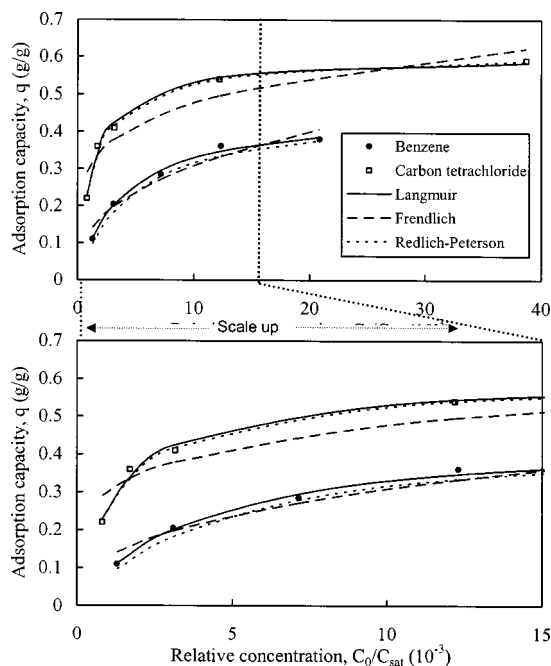
VOC	Conditions and result	Unit	Run 1	Run 2	Run 3	Run 4	Run 5
C <sub>6</sub> H <sub>6</sub>	Concentration, C <sub>0</sub>	mmol/m <sup>3</sup>	8.1	19.5	45.1	77.7	131.6
	Activated carbon weight, W	g	2.002	2.005	2.002	2.011	2.005
	Equilibrium adsorption weight, W <sub>e</sub>	mmol	2.82	5.26	7.31	9.32	9.79
	Equilibrium adsorption capacity, q	mg/g	110	205	285	362	381
CCl <sub>4</sub>	Concentration, C <sub>0</sub>	mmol/m <sup>3</sup>	6.1	12.8	23.7	91.7	291.1
	Activated carbon weight, W	g	0.601	0.600	0.600	1.000	2.000
	Equilibrium adsorption weight, W <sub>e</sub>	mmol	0.86	1.40	1.60	3.50	7.66
	Equilibrium adsorption capacity, q	mg/g	220	360	410	539	590

Note: Experimental condition: T=303 K and Q=1.2 L/min.

and adsorbate (1/K), but also provides a guideline for predicting the service time during the adsorption cycle.

Table 5 and Fig. 6 compare the equilibrium adsorption constants obtained from the Langmuir adsorption isotherm and model calculations. Results show that the average relative percentage difference (RPD) value is about 6%, which indicates that the model predicated well the adsorption and desorption rate constants.

Vahdat (1997) reported Langmuir constants between 27 VOCs and 11 activated carbons and suggested that both the VOCs and activated carbon can affect the Langmuir constants (q<sub>0</sub> and K<sub>L</sub>). For benzene, the average q<sub>0</sub> is 0.353 g/g; the average K<sub>L</sub> is 60.1 m<sup>3</sup>/mol; the maximum K<sub>L</sub> is 120.2 m<sup>3</sup>/mol; and the minimum K<sub>L</sub> is 34.5 m<sup>3</sup>/mol at 298 K. For carbon tetrachloride, the average q<sub>0</sub> is 0.738 g/g; the average K<sub>L</sub> is 61.3 m<sup>3</sup>/mol; the maximum K<sub>L</sub> is 163.7 m<sup>3</sup>/mol; and the minimum K<sub>L</sub> is 43.3 m<sup>3</sup>/mol in the temperature range of 296–298 K. In a previous study, Chiang et al. (2001) reported a q<sub>0</sub> of 0.43 and 0.62 g/g for benzene and carbon tetrachloride, individually, and a K<sub>L</sub> of 29 and 90 m<sup>3</sup>/mol for benzene and carbon tetrachloride, respectively, at 300 K for the same activated carbon sample (Fig. 6). Our results of Langmuir constants were of the same order of magnitude as those reported by Vahdat (1997) and Chiang et al. (2001).

**Fig. 4.** Adsorption isotherms of C<sub>6</sub>H<sub>6</sub> and CCl<sub>4</sub> at 303 K

### Effect of Temperature and Concentration

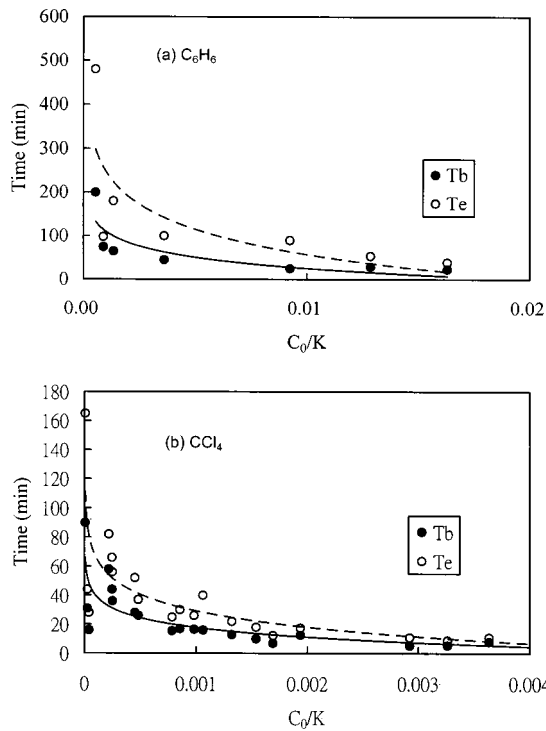
Fig. 7 illustrates the effect of temperature on the adsorption of VOCs. Results indicate that the adsorption of C<sub>6</sub>H<sub>6</sub> was not temperature dependent, especially in the low VOC concentration range. As relative concentration increased, the effect of temperature on VOC adsorption diminished.

Fig. 8 shows predicted single-contaminant breakthrough curve as a function of temperature. For the single contaminant system, the model predicts well the adsorption breakthrough curves of both C<sub>6</sub>H<sub>6</sub> and CCl<sub>4</sub>. At high reaction temperatures, the adsorption capacity decreased due in part to small equilibrium constants and an early breakthrough time. The breakthrough curves were steeper at high temperatures than at low temperatures, due in part to the effects of k<sub>a</sub> and k<sub>d</sub>. Furthermore, CCl<sub>4</sub> has a longer relative breakthrough time, due to low inlet CCl<sub>4</sub> concentrations.

Fig. 9 shows the predicted breakthrough curves of the binary contaminant system at four temperatures. The inlet concentrations of CCl<sub>4</sub> at 303, 323, 343, and 363 K were 1.26×10<sup>-2</sup>, 1.45×10<sup>-2</sup>, 1.54×10<sup>-2</sup>, and 3.07×10<sup>-2</sup> mol/m<sup>3</sup>, respectively;

**Table 4.** Pertinent Parameters of Various Adsorption Isotherm Equations

VOC	Isotherm	Parameter	Unit	Value	
C <sub>6</sub> H <sub>6</sub> (N=5)	Langmuir	q <sub>0</sub>	g/g	0.46	
		$q = \frac{q_0 K_L C}{1 + K_L C}$	K <sub>L</sub>	m <sup>3</sup> /mol	39.8
		R <sup>2</sup>	—	0.99	
	Freundlich	$q = K_F C^n$	K <sub>F</sub>	g/g	0.88
		R <sup>2</sup>	—	0.97	
	Redlich–Peterson	$q = \frac{K_R C}{B + C^m}$	K <sub>R</sub>	mol/m <sup>3</sup>	0.44
			B	—	0.03
m		—	1.03		
R <sup>2</sup>	—	0.99			
CCl <sub>4</sub> (N=5)	Langmuir	q <sub>0</sub>	g/g	0.60	
		$q = \frac{q_0 K_L C}{1 + K_L C}$	K <sub>L</sub>	m <sup>3</sup> /mol	99.8
		R <sup>2</sup>	—	0.99	
	Freundlich	$q = K_F C^n$	K <sub>F</sub>	g/g	0.80
		R <sup>2</sup>	—	0.89	
	Redlich–Peterson	$q = \frac{K_R C}{B + C^m}$	K <sub>R</sub>	mol/m <sup>3</sup>	0.62
			B	—	0.01
m		—	0.98		
R <sup>2</sup>	—	0.99			



**Fig. 5.** Relationship of inlet concentration with equilibrium constant and breakthrough time or equilibrium time ( $W=2.0$  and  $0.6$  g for  $C_6H_6$  and  $CCl_4$ , respectively)

whereas the inlet concentrations of  $C_6H_6$  were  $6.38 \times 10^{-2}$ ,  $6.86 \times 10^{-2}$ ,  $7.84 \times 10^{-2}$ , and  $1.64 \times 10^{-1}$  mol/m<sup>3</sup>, individually. In general, the predicted results agree well with what were observed. Again, high temperatures exhibited a steeper breakthrough curve and an earlier breakthrough time. At high temperatures, the adsorption and desorption rate constants were large, whereas the equilibrium constants were small. Both high adsorption and desorption rate constants were typically related to steeper breakthrough curves, whereas low equilibrium constants cause low adsorption density and early breakthrough time.

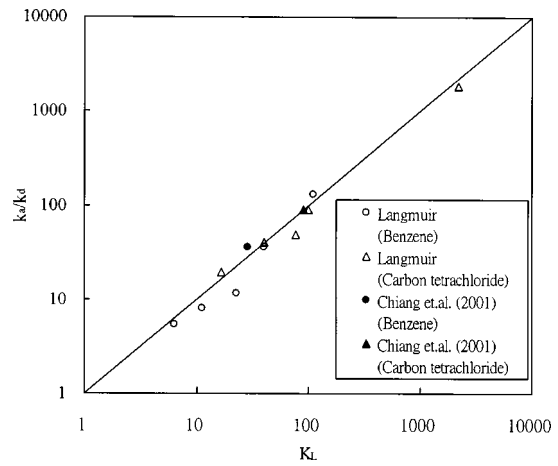


**Fig. 6.** Relationship of equilibrium constants of Langmuir and adsorption/desorption models

Fig. 10 shows the predicted results at three concentration level of VOC, i.e., high ( $[C_6H_6]_0 = 309$  mmol/m<sup>3</sup>,  $[CCl_4]_0 = 90$  mmol/m<sup>3</sup>); medium ( $[C_6H_6]_0 = 164$  mmol/m<sup>3</sup>,  $[CCl_4]_0 = 31$  mmol/m<sup>3</sup>); and low ( $[C_6H_6]_0 = 84$  mmol/m<sup>3</sup>,  $[CCl_4]_0 = 16$  mmol/m<sup>3</sup>) concentrations. At the high (or medium) inlet concentration, the effluent concentration ratio ( $C/C_0$ ) of the weak adsorbate ( $C_6H_6$ ) presents a high  $C/C_0$  value (1.20 versus 1.06 for  $CCl_4$ ) when the breakthrough time approaches 30 min (versus 55 min for  $CCl_4$ ). At a high inlet concentration, the strong adsorbate competed with the weak adsorbate, and caused the desorption rate of the weak adsorbate to be higher than the adsorption rate. It caused the outlet concentration to be higher than the inlet concentration ( $C_0$ ). However, the effluent concentration ratio of  $C_6H_6$  did not exhibit a value higher than 1.0 at the low concentration level. The total adsorption capacity of  $C_6H_6$  and  $CCl_4$  was found to decrease as the inlet concentration decreased.

It was thus concluded that, at high temperature and/or high inlet concentration, there was significant adsorptive breakthrough. For both high-inlet concentration (Fig. 10) and low-temperature conditions (Fig. 9), the weak adsorbate,  $C_6H_6$ , exhibited a high adsorption density at the beginning of the experiment.

**Table 5.** Relationships of Equilibrium Constants of Both Langmuir and Adsorption/Desorption Models

VOC	Parameter	Unit	Temperature					
			Temp. (K)	283	303	323	343	363
$C_6H_6$	Number of test	$N$	—	3	5	3	3	3
	Langmuir	$q_0$	g/g	0.46 <sup>a</sup>	0.46	0.46 <sup>a</sup>	0.46 <sup>a</sup>	0.46 <sup>a</sup>
		$K_L$	m <sup>3</sup> /mol	111.5	39.8	22.5	11.2	6.3
		$R^2$	—	0.97	0.99	0.54	0.68	0.72
	Ads./Des.	$K$	m <sup>3</sup> /mol	130.0	36.6	11.7	8.0	5.4
	Statistics	RPD <sup>b</sup>	%	3.8	2.1	15.8	8.3	3.7
$CCl_4$	Number of test	$N$	—	3	5	5	5	4
	Langmuir	$q_0$	g/g	0.60 <sup>a</sup>	0.60	0.60 <sup>a</sup>	0.60 <sup>a</sup>	0.60 <sup>a</sup>
		$K_L$	m <sup>3</sup> /mol	2,212	99.8	78.0	40.4	16.7
		$R^2$	—	0.72	0.99	0.79	0.57	0.60
	Ads./Des.	$K$	m <sup>3</sup> /mol	1,875	90.0	50.0	41.7	19.4
	Statistics	RPD <sup>b</sup>	%	4.1	2.6	11.0	0.8	3.7

<sup>a</sup>Fixed at the same value of 303 K.

<sup>b</sup>RPD =  $|K_L - K| / 2(K_L + K)$ .

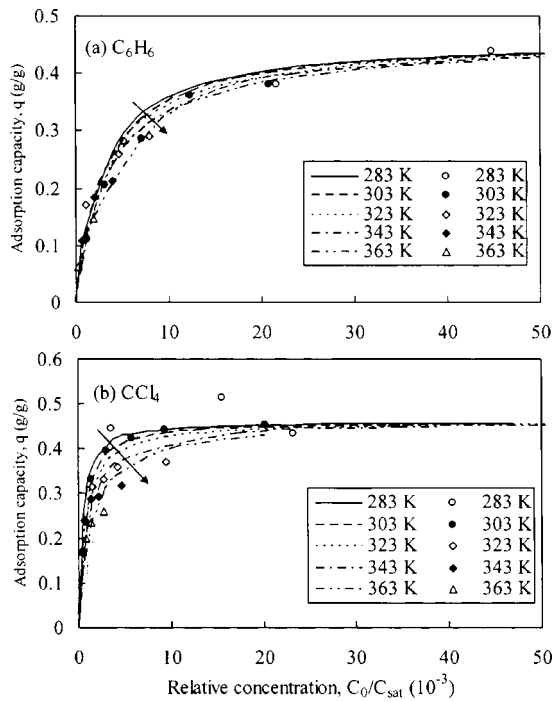


**Fig. 7.** Prediction of adsorption isotherms under different concentration and temperature conditions (points are experimental data and lines are model predicted)

Binary contaminant breakthrough shows a competitive adsorption. For example, at 303 K, with  $\text{CCl}_4$  and  $\text{C}_6\text{H}_6$  inlet concentrations of  $1.26 \times 10^{-2}$  and  $6.38 \times 10^{-2} \text{ mol/m}^3$ , the experimental adsorption capacities are about 1.8 and 2.0 mol/kg, respectively. For a single contaminant adsorption, the adsorption of  $\text{CCl}_4$  and  $\text{C}_6\text{H}_6$  are 2.9 and 4.2 mol/kg, respectively. As expected, at binary

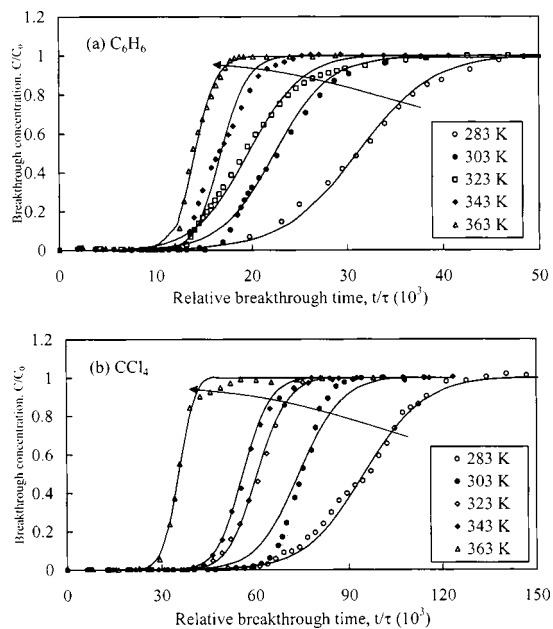


**Fig. 8.** Prediction of volatile organic compound breakthrough as function of temperature (points are experimental data and lines are model predicted, influent concentrations of  $\text{C}_6\text{H}_6$  and  $\text{CCl}_4$  are 88–132 and 20–27 mmol/m<sup>3</sup>, respectively)

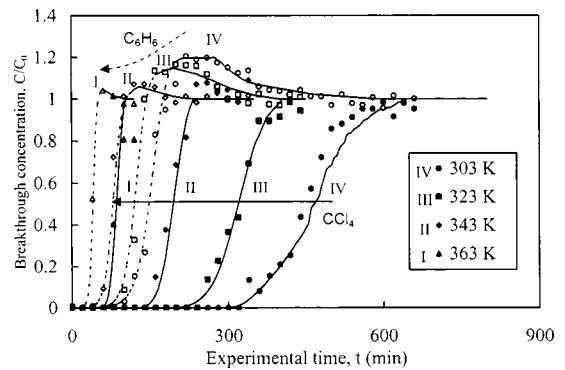


**Fig. 9.** Prediction of binary adsorption breakthrough curves under different temperature conditions (solid points are experimental  $\text{CCl}_4$  data, air-corn points are experimental  $\text{C}_6\text{H}_6$  data, solid lines are predicted  $\text{CCl}_4$  value, and broken lines are predicted  $\text{C}_6\text{H}_6$  value,  $W = 4.0 \text{ g}$ )

contaminant adsorption, the adsorption capacities are smaller than that of a single contaminant adsorption.

## Conclusion

The activated carbon adsorption process was affected by several factors, such as temperature, adsorbent and adsorbate characteristics, and VOC concentration. In this study, a numerical model was developed. Results show that model-fitted adsorption and desorption rate constants could predict well the adsorption isotherms and breakthrough curves under various conditions. Both experimental and model-predicted data indicate that under high reaction temperatures, both the adsorption and desorption rate constants increase, whereas equilibrium adsorption constants decreased. The adsorption capacity was also affected by temperature. For binary contaminants adsorption, a high inlet concentration or a low temperature will cause a high breakthrough concentration of weak adsorbate ( $\text{C}_6\text{H}_6$ ) when contaminant ( $\text{CCl}_4$ ), a strong adsorbate, began to break through.

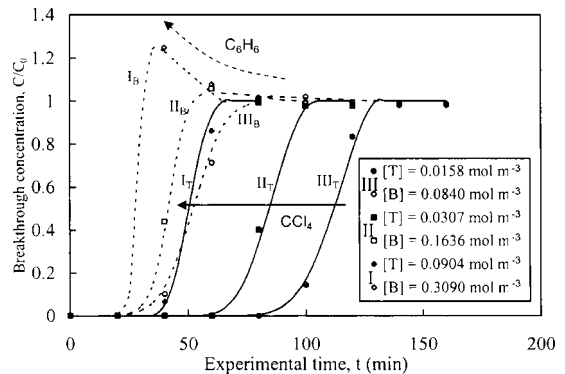


**Fig. 10.** Prediction of binary adsorption breakthrough curves under different concentration conditions (363 K,  $W = 4.0 \text{ g}$ , solid points are experimental  $\text{CCl}_4$  data, air-corn points are experimental  $\text{C}_6\text{H}_6$  data, [T] and [B] are concentration (mol/m<sup>3</sup>) of carbon tetrachloride and benzene)

## References

- Chiang, Y. C., Chiang, P. C., and Chang, E. E. (2001). "Effects of surface characteristics of activated carbons on VOC adsorption." *J. Environ. Eng.*, 127, 54–62.
- Crittenden, J. C., and Weber, W. J. (1978). "Predictive model for design of fixed-bed adsorbers: single-component model verification." *J. Environ. Eng.*, 104, 433–443.
- Dubinin, M. M. (1989). "Fundamentals of the theory of adsorption in micropores of carbon adsorbents: characteristics of their adsorption properties and microporous structures." *Carbon*, 27, 457–467.
- Jonas, L. A., and Rehmann, J. A. (1972). "The kinetics of adsorption of organo-phosphorus vapors from air mixtures by activated carbon." *Carbon*, 10, 657–663.
- King, B., and Do, D. D. (1996). "Measurement of multicomponent adsorption kinetics of gases in activated carbon by a batch adsorber FT-IR technique." *Chem. Eng. Sci.*, 51, 423–439.
- Malek, A., and Farooq, S. (1996). "Comparison of isotherm models for hydrocarbon adsorption on activated carbon." *AIChE J.*, 42, 3191–3201.
- Malek, A., and Farooq, S. (1997). "Kinetics of hydrocarbon adsorption on activated carbon and silica gel." *AIChE J.*, 43, 761–776.
- Malek, A., Farooq, S., Rathor, M. N., and Hidajat, K. (1995). "Effect of velocity variation due to adsorption-desorption on equilibrium data from breakthrough experiments." *Chem. Eng. Sci.*, 50, 737–740.
- Myers, A. L., and Prausnitz, J. M. (1965). "Thermodynamics of mixed-gas adsorption." *AIChE J.*, 11, 121–126.
- Myers, A. L., and Valenzuela, D. P. (1986). "Computer algorithm and graphical method for calculating adsorption equilibria of gas mixtures." *J. Chem. Eng. Jpn.*, 19, 392–396.
- Pigram, P. J., Lamb, R. N., Hibbert, D. B., and Collins, R. E. (1994). "Modeling of the desorption behavior of microporous amorphous hydrogenated carbon films." *Langmuir*, 10, 142–147.
- Vahdat, N. (1997). "Theoretical study of the performance of activated carbon: in the presence of binary vapor mixtures." *Carbon*, 35, 1545–1557.
- Vahdat, N., Swearingen, P. M., Johnson, J. S., Priante, S., Mathews, K., and Neihart, A. (1995). "Adsorption capacity and thermal desorption efficiency of selected adsorbents." *Am. Ind. Hyg. Assoc. J.*, 56, 32–38.
- Wood, G. O. (1992). "Activated carbon adsorption capacities for vapors." *Carbon*, 30, 593–599.
- Yoon, Y. H., and Nelson, J. H. (1984). "Application of gas adsorption kinetics: I. A theoretical model for respirator cartridge service life." *Am. Ind. Hyg. Assoc. J.*, 45, 509–516.